Piezoelectric Thin Films of ZnO-Nanorods/Nanowalls Grown by Chemical Bath Deposition

Marco Fortunato, *Member, IEEE*, Chandrakanth Reddy Chandraiahgari, Giovanni De Bellis, *Member, IEEE*, Paolo Ballirano, Peiman Soltani, Saulius Kaciulis, Luisa Caneve, Francesca Sarto, and Maria Sabrina Sarto, *Fellow, IEEE*

***Abstract*—This study presents a comparison of the piezoelectric properties of nanostructured thin films made of arrays of vertically oriented ZnO-nanorods (ZnO-NRs) over ITO-glass substrate and of ZnO-nanowalls (ZnO-NWs) over aluminium substrate. Both nanostructures were synthesized on a large area through chemical bath deposition. The morphological, structural, and chemical characteristics of the produced nanostructures were investigated in order to assess the crystal quality and purity. To this purpose, we used different techniques, such as field-emission scanning electron microscopy, atomic force microscopy, energy dispersive x-ray analysis, powder x-ray diffraction, x-ray photoelectron spectroscopy, and photoluminescence spectroscopy. Moreover, the piezoelectric response of the nanostructured films was assessed through piezoresponse force microscopy. This technique was employed to obtain a quantitative evaluation of the piezoelectric coefficient (d_{33}) of the film. We obtained d_{33} values as high as (7.01 $\pm$ 0.33) pm/V for ZnO-NRs and (2.63 $\pm$ 0.49) pm/V for ZnO-NWs films.**

***Index Terms*—Piezoresponse force microscopy (PFM), ZnO nanorods (NRs), ZnO nanowalls (NWs), chemical bath deposition (CBD), piezoelectric coefficient (d_{33}).**

I. Introduction

ZINC oxide (ZnO) has been attracting a great deal of interest from the scientific community over the last decades, owing to a variety of intriguing properties, along with a remarkable performance for several applications, such as piezoelectric transducers, photovoltaic devices, gas and bio-sensors, nanoscale optoelectronics and self-powered micro/nanosystems, [1]–[5]. ZnO is an n-type semiconductor with a wide energy gap (3.37 eV), high exciton binding energy (60 meV), high electron mobility, and unique optical, pyroelectric, and piezoelectric properties [6]. It crystallizes preferentially in the hexagonal wurtzite-type structure and forms a rich variety of nanostructures. In the last years, ZnO nanostructures have stimulated also a considerable appeal owing to their excellent biocompatibility [7].

Several methods have been developed to grow ZnO nanostructures [8]–[13]. Among them chemical bath deposition (CBD) [10]–[12] has received much attention, as it ensures a high deposition rate on a wide variety of substrates; moreover, it is facile, cost-effective and easy to scale-up. The properties of ZnO nanostructures are strongly dependent on their size, shape, and morphology [11], [14]–[16]. In particular, the characterization of the piezoelectric properties of ZnO nanostructures having different morphology is a fundamental step towards the production and performance optimization of nano-generators and nano-actuators.

An extensive overview of piezoelectric measurement techniques is reported in [17]. Among state-of-art measurement methods, the Piezoresponse Force Microscopy (PFM) is one of the most widely used techniques for the characterization of piezoelectric nanostructures, since it enables the measurement of the piezo-displacement with pico-meter resolution [18]. A conductive tip is used, as a movable top electrode, to apply a voltage to the sample, causing strains due to the inverse piezoelectric effect [19]. Since the induced local displacement is related to the local value of the piezoelectric coefficient of the material, PFM can provide a quantitative information [18], [20]. PFM is a non-disrupting test method since it does not require sample metallization nor top-electrode deposition over the material under test.

However, the main limitation of this technique is that it provides typically a local characterization of the piezoresponse of the material under test. In [21] and [22], the piezoelectric coefficient was measured locally through PFM by scanning single piezoelectric domains and then averaging. Therefore, the obtained d_{33} represents an overestimation of the piezoresponse of the material at macroscale.

Manuscript received November 6, 2017; revised December 22, 2017; accepted January 24, 2018. Date of publication January 31, 2018; date of current version March 8, 2018. The review of this paper was arranged by associate editor Y. Hu. *(Corresponding author: Marco Fortunato.)*

M. Fortunato, C. R. Chandraiahgari, G. De Bellis, and M. S. Sarto are with the Department of Astronautical, Electrical and Energy Engineering, Sapienza University of Rome, Rome 00154, Italy, and also with the Research Center for Nanotechnology Applied to Engineering, Sapienza University of Rome, Rome 00185, Italy (e-mail: marco.fortunato@uniroma1.it; chandra.nano@gmail.com; giovanni.debellis@uniroma1.it; mariasabrina.sarto@uniroma1.it).

P. Ballirano is with the Department of Earth Sciences, Sapienza University of Rome, Rome 00185, Italy (e-mail: paolo.ballirano@uniroma1.it).

P. Soltani and S. Kaciulis are with the CNR-ISMN, Monterotondo 00015, Italy (e-mail: peiman.soltani@ismn.cnr.it; saulius.kaciulis@ismn.cnr.it).

L. Caneve and F. Sarto are with the ENEA, Frascati Research Center, Rome 00044, Italy (e-mail: luisa.caneve@enea.it; francesca.sarto@enea.it).

Digital Object Identifier 10.1109/TNANO.2018.2800406

In this paper, we propose the use of PFM to quantitatively evaluate the effective piezoelectric coefficient d_{33} of nanostructured thin films. To this purpose, the PFM signal is averaged over an area which is much larger than the tip curvature radius and the size of the piezoelectric domains. Therefore, the proposed approach could be implemented as a routine test for quality-control of nanostructured piezoelectric materials before device assembling. We also perform a complete characterization of the produced nanostructures through several techniques (i.e., Field Emission Scanning Electron Microscopy - FE-SEM, Energy Dispersive X-ray analysis - EDX, Atomic Force Microscopy - AFM, Powder X-Ray Diffraction - P-XRD, X-ray Photoelectron Spectroscopy - XPS, Photoluminescence Spectroscopy - PL), in order to correlate the piezoresponse of the nanostructured films with the structural, chemical and morphological properties of the nanostructures (ZnO-NRs and ZnO-NWs).

II. Experimental

Large arrays of vertically aligned ZnO-NRs over Indium Tin Oxide coated glass substrated (ITO/G) and of ZnO-NWs over aluminium foil (Al-foil) were produced starting from zinc acetate precursors through the CBD technique.

A. Materials

All chemicals were of reagent grade and used as received: zinc acetate dihydrate ($Zn(CH_3COO)_2 \cdot 2H_2O$, Sigma-Aldrich, ≥98%), zinc nitrate hexahydrate ($Zn(NO_3)_2 \cdot 6H_2O$, Acros Organics, 98%), hexamethylenetetramine ($C_6H_{12}N_4$, Fisher Scientific, ≥99%), isopropanol ($(CH_3)_2CHOH$, Sigma-Aldrich, ACS reagent, ≥99%), acetone (CH_3COCH_3, Acros Organics, ≥99%) and deionized water (DI) with a resistivity of 18 MΩ·cm. Indium tin oxide coated (∼100 nm) glass slides (ITO/G: ∼1.1 mm thick) and aluminium foil (Al-foil: ∼25 μm thick) were purchased from Sigma-Aldrich and used as substrates.

B. Synthesis

The growth substrates (i.e., ITO/G for ZnO-NRs and Al-foil for ZnO-NWs) were first cleaned in acetone and then in isopropanol. Subsequently they were dried in an oven at 70 °C for 10 min. Prior to the growth, a seed layer was deposited onto the cleaned substrates by the dip-coating method. A seed solution was prepared by dissolving 5 mM of zinc acetate dehydrate in to 40 ml of isopropanol using magnetic stirring at room temperature. The substrates were then dip-coated in the seed solution and underwent thermal annealing inside a muffle furnace at 300 °C for 30 min. This process resulted in substrates coated uniformly with ZnO seed particles having an average diameter of 20 nm [23]. ZnO nanostructures were grown on the seeded substrates using the facile CBD described in our earlier work [23]. Briefly, an aqueous growth solution was prepared by dissolving 20 mM equimolar ratios of zinc nitrate hexahydrate and hexamine together in 100 ml of DI water. The seeded substrate was then horizontally suspended upside-down into the growth solution. The suspension was placed on a hot plate (Heidolph MR-Hei Standard) under static conditions for 4.5 h. During the reaction, the beaker was sealed with an Al foil and the solution temperature was fixed at 60 °C using an automatic electronic temperature controller (EKT Hei-Con). After the growth reaction, the substrate was removed from the solution, rinsed in DI water and dried in oven at 120 °C for 30 min. At the end of the process ZnO-NRs or ZnO-NWs were grown, depending on the seeded substrate used (ITO/G or Al-foil, respectively).

C. Characterization

The morphology of the ZnO nanostructures was investigated through FE-SEM (Zeiss Auriga) and AFM (Bruker-Veeco Dimension Icon). In particular, FE-SEM images were used to estimate the lateral size of the ZnO-NRs and ZnO-NWs and the thickness of ZnO-NWs, while the height of the nanostructures was assessed through tapping mode AFM scan.

Chemical composition analysis was performed through EDX using the FE-SEM, Zeiss Auriga, equipped with a Bruker Quantax EDX capable of an energy resolution of 123 eV at Mn Kα.

The structural characterization and phase identification of the synthesized ZnO nanostructures were performed through P-XRD in transmission mode on a focusing beam Bruker AXS D8 Advance diffractometer using CuKα radiation ($\lambda = 0.15418$ nm), operating at 40 kV and 40 mA. Data were collected in a 2θ angular range extending from 20° to 145° with a step size 0.022° and 1 s counting time. The instrument is fitted with incident-beam Göbel mirrors and a position sensitive detector VÅntec. Samples were prepared as capillaries loaded with respective nanostructures in powder form obtained upon removal from the growth substrate by using bath sonication. A preliminary check was done using a Siemens D5000, operating in reflection mode, using CuKα radiation ($\lambda = 0.15418$ nm), operating at 40 kV and 40 mA. Analyses pointed out the presence of ZnO under the hexagonal wurtzite modification. Structural refinements were performed by the Rietveld method using TOPAS v.4.2 (Bruker AXS 2009) software. Details of the refinement procedure can be found in reference [10].

XPS was performed using a monochromatized spectrometer Escalab 250Xi (Thermo Fisher Scientific, UK) equipped with a six-channeltron detection system for spectroscopy. The samples were loaded in an ultra-high vacuum (UHV) chamber, using the Al Kα X-ray source set to the diameter of 900 μm, the analyzer at a constant pass energy of 20 eV, and the standard mode of electromagnetic input lenses (about 1 mm in diameter). The acquired data were processed by the Avantage v.5 software (Thermo Fisher Scientific, UK).

The photoluminescence (PL) spectra of both ZnO-NRs and ZnO-NWs were recorded at room temperature by using the 266 nm line of a Nd:YAG pulsed laser (Thomson DIVA) as the exciting source, having 10 ns pulse length and 20 Hz repetition rate. Further details on the PL experimental setup and procedure can be found in [10]. Spectra were repeated on the same sample 16 times and averaged to get proper statistics. The measurements were performed at different power levels of the exciting laser in the range 700–1300 W/m^2, in order to discriminate between linear and non-linear behaviour of the defect-related and band

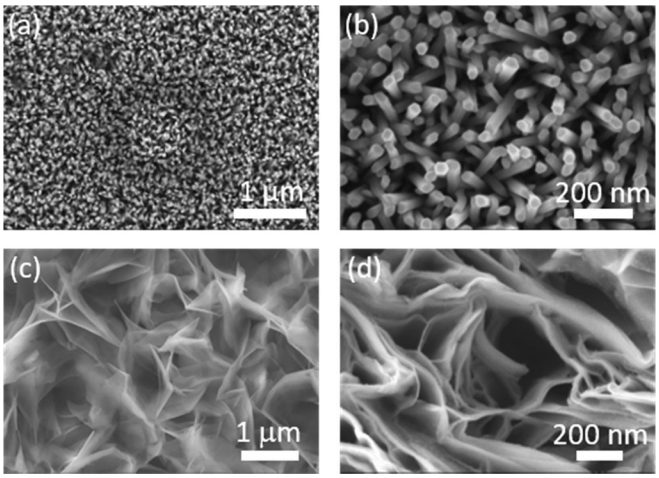

Fig. 1. FE-SEM micrographs of ZnO-NRs and ZnO-NWs at low magnification (25 kX and 50 kX respectively) (a), (c) and at high magnification (100 kX and 200 kX, respectively) (b), (d).

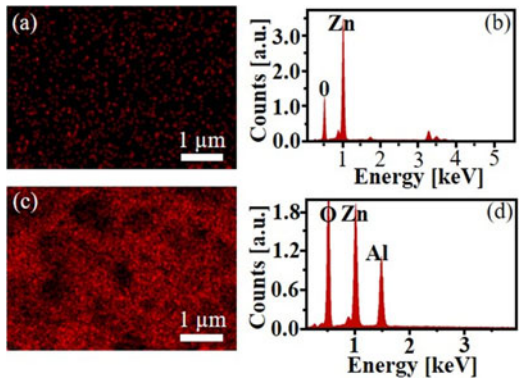

Fig. 2. EDX elemental Zn mapping in (a) ZnO-NRs and (c) ZnO-NWs samples. EDX spectra of (b) ZnO-NRs and (d) ZnO-NWs.

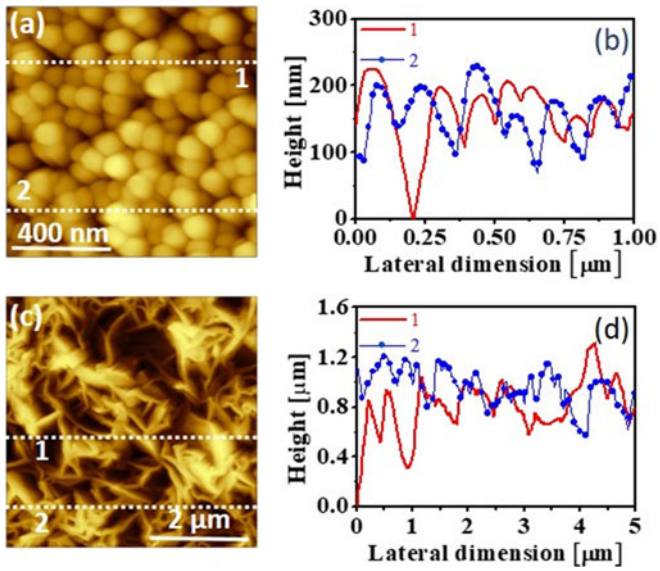

Fig. 3. AFM topography in tapping mode of (a) ZnO-NRs and (c) ZnO-NWs, height profile along the red and blue lines for (b) ZnO-NRs and (d) ZnO-NWs.

edge PL emissions. Since the ZnO-NRs and ZnO-NWs samples were grown on different substrates, the spectra of bare ITO/glass and Al-foil substrates were also acquired for reference, and used to correct the spectra of the ZnO-NRs and ZnO-NWs samples.

PFM measurements were performed using a commercial Bruker-Veeco Dimension Icon AFM, equipped with the piezoelectric module under the following conditions: silicon cantilever (Bruker) with 115-135 μm length, nominal spring constant of 5 N/m, Co-Cr coated tip with electrical resistivity of 0.01–0.025 $\Omega\cdot$cm, tip curvature radius $\sim$35 nm and nominal resonance frequency of 150 kHz. In order to measure the piezoresponse of the samples, an a.c. voltage was applied to the tip, with amplitude varying from 4 mV to 5 V at a fixed frequency of 17 kHz. Scan rate was 0.5 Hz and the scan area was $(600 \times 600)\,\text{nm}^2$. Three different areas were scanned for each sample and the measured data were averaged. All measurements were performed in an insulating chamber to avoid acoustic excitation.

III. Results and Discussion

A. FE-SEM, AFM and EDX Characterizations

The morphology of ZnO-NRs and ZnO-NWs, as observed through FE-SEM, is shown in Fig. 1(a)–(d).

The vertical alignment of ZnO-NRs can be observed in Fig. 1(a) and (b), highlighting a very narrow size distribution of the nanostructures with estimated diameter of $(\sim 42 \pm 5)$ nm.

ZnO-NWs are characterized by thin walls with very sharp edges (Fig. 1(c) and (d)). The thickness and lateral size of ZnO-NWs are evaluated as $(\sim 38 \pm 28)$ nm and $(\sim 950 \pm 370)$ nm, respectively.

The EDX analysis performed on ZnO-NRs (Fig. 2(a) and (b)) shows an excess of Zn, and a few small peaks originated by the ITO/G substrate. The excess of Zn implies a non-stoichiometric Zn/O ratio. The compositional Zn map, reported in Fig. 2(a), shows a homogenous distribution of Zn over the ZnO-NRs structures.

The EDX analysis of ZnO-NWs (Fig. 2(c) and (d)), shows equally intense O and Zn peaks, together with the peak produced by the Al substrate. Moreover, we observe a slight excess of oxygen, leading to a non-stoichiometric Zn/O ratio. The Zn compositional map, reported in 2(c), shows also for ZnO-NWs a homogenous distribution.

AFM measurements, performed in tapping mode, are shown in Fig. 3(a) and (c).

Height measurements, evaluated through AFM, resulted in values of $(\sim 150 \pm 80)$ nm for ZnO-NRs and $(\sim 890 \pm 510)$ nm for ZnO-NWs, as deduced from the reported signal profiles, averaged along the scanned area (see Fig. 3(b) for ZnO-NRs and 3(d) for ZnO-NWs). It is noted that these measurements represent a qualitative indication of the height of the structures, due to the error stemming from the convolution of the real morphology and the tip shape, resulting in a curvature radius of the tip comparable with the diameter of the nanostructures under analysis. Nevertheless, we can say that the morphology of the nanostructures produced are characterized by truly different

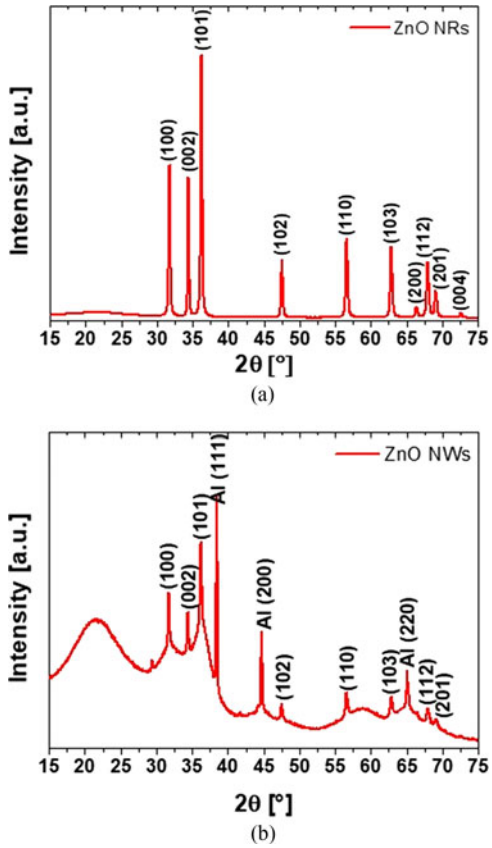

Fig. 4. X-ray diffraction (XRD) pattern acquired on (a) ZnO-NRs and (b) ZnO-NWs.

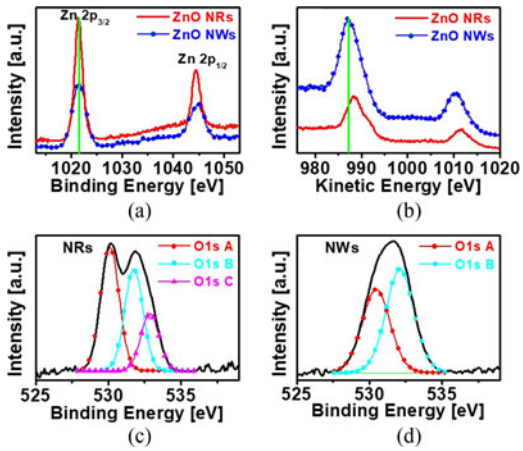

Fig. 5. (a) Zn 2p spectra and (b) Zn LMM spectra of ZnO-NRs and ZnO-NWs, O1s spectra of (c) ZnO-NRs and (d) ZnO-NWs.

aspect ratio (i.e., height over radius or wall thickness): $\sim$4 for ZnO-NRs and $\sim$23 for ZnO-NWs.

B. XRD Analysis

The crystallinity of the ZnO-NRs and ZnO-NWs powders was evaluated by XRD analysis. Fig. 4(a) and (b) show the powder XRD pattern of the ZnO-NRs and ZnO-NWs, respectively.

The sharp and intense peaks, which are observed for both samples, indicate the highly crystalline nature of the produced ZnO nanostructures. However, the spectrum observed for ZnO-NWs, contains some peaks referable to Al, used as the growth substrate, and a strong broad band centred around 21.7° which arises from the glass capillary. Furthermore, for the same sample, an anomalous spread of some peaks is observed at the base of the pattern. We suppose that such an anomalous behaviour can be ascribed to the presence of high defectivity, which is further investigated using photoluminescence and discussed in the subsequent section.

ZnO-NRs are characterized by cell parameters and bond distances very similar to those reported for other nanorods samples [10]. In particular, the cell volume of 47.6318(3) Å^3 is higher than the one reported for bulk ZnO [24]. This behaviour agrees with that reported for other simple oxides, whose cell parameters and volume of the bulk material are smaller than those of micro- and nano-structured equivalents [25]–[27]. The <Zn-O> bond distance is of 1.978 Å and the ZnO_4 tetrahedron is slightly distorted as a result of $3 \times 1.9753(3)$ Å and $1 \times 1.9864(12)$ Å bond distances. ZnO-NRs has an ε_0 micro-strain (lattice strain), defined as $\beta_i = 4\varepsilon_0 \tan\theta$, β_i being the peak integral breadth, of 0.0376(5). Differently, ZnO-NWs are characterized by a significantly broadened peak shape that was impossible to properly fit even applying the ellipsoid-model of Katerinopoulou *et al.* [28], describing the diffraction-vector dependent broadening of diffraction maxima. This is clearly due to extended defectivity of the material. This fact is confirmed by a unit cell volume of 47.565(8) Å^3 smaller than that found in bulk ZnO (47.598(7) Å^3). In particular, Kaurova *et al.* [29] indicated that the occurrence of O-vacancies is coupled to a marked reduction of the cell parameters. Moreover, we investigated the possible symmetry reduction from $P6_3/mc$, which is typical of stoichiometric zincite, to *P*3, which has been observed in O-defective samples [29]. No Bragg reflection at ca. 17.2° 2θ was observed, attributed to the symmetry-violating 001 peak by those authors, indicating that the correct space group for ZnO-NWs is $P6_3/mc$. Coherently, the ε_0 micro-strain was 0.0901(15) significantly higher than that of ZnO-NRs. Due to the imperfect peak shape fit, bond distances were not refined [21]. The hypothesis of a significant defectivity of ZnO-NWs is further supported by PL measurements, as discussed in the following.

C. XPS Characterization

The surface chemical composition of ZnO-NRs and ZnO-NWs has been analysed by XPS. In all samples, Zinc is present in the Zn(+2) chemical state, which is evident from the binding-energy (BE) value of the Zn $2p_{3/2}$ peak at 1021.4 eV for ZnO-NRs and at 1021.5 eV for ZnO-NWs (Fig. 5(a)) and from the Auger Zn LMM peak position at a kinetic energy (KE) of $\sim$988.5 eV for ZnO-NRs and of $\sim$987.2 eV for ZnO-NWs (Fig. 5(b)) [30], [31]. In addition, the values of the modified Auger parameter $\alpha \approx 2009.9$ eV for ZnO-NRs and $\alpha \approx 2008.7$ eV for ZnO-NWs, correspond to the Zn(+2) chemical state [30], [32]. The spectra of Zn 2p and Zn LMM regions

TABLE I
XPS ELEMENTAL QUANTIFICATION

Sample	Peak	BE (eV)	Atomic %	Chemical State
ZnO-NRs	O1s A	530.1	28.5	ZnO
	O1s B	531.8	23.4	OH^-
	O1s C	532.9	13.2	H_2O
	$Zn2p_{3/2}$	1021.4	34.9	ZnO
ZnO-NWs	O1s A	530.5	32.6	ZnO
	O1s B	532.1	40.5	OH^-
	$Zn2p_{3/2}$	1021.5	26.9	ZnO

are shown in Fig. 5(a) and (b), respectively. The O1s spectra of ZnO-NRs, shown in Fig. 5(c), consists of three components indicated as O1sA, O1sB and O1sC. Differently, the O1s spectra of ZnO-NWs, shown in Fig. 5(d), consists of two components indicated as O1sA and O1sB. The first component is attributed to O^{2-} ions in the wurtzite structure of ZnO, whereas the second one is attributed to the loosely bound oxygen on the surface, such as in adsorbed hydroxyl groups -OH and/or -CO3 radicals [30], [33]. The third components at BE $\approx$ 533 eV is due to the water molecules absorbed on the sample surface. XPS quantification was done by using Shirley background subtraction and a standard set of Scofield sensitivity factors. The surface contaminants (C and N) were not included in this quantification. The obtained results are summarized in Table I.

The O1s spectra of both samples including the peak fitting are presented in Fig. 5(c) and (d). To better understand the differences between the samples, the ratio of Zn to O was computed for the component of oxide O 1s A. In the case of Zn/O $>$ 1, the lack of oxygen is an indicator of a higher number of defects in zinc oxide. For ZnO-NRs, the Zn/O ratio was equal to 1.2, whereas for ZnO-NWs it was 0.82.

These results are in good agreement with the results of EDX and PL measurements (shown in the next paragraph), confirming an excess of Zn in ZnO-NRs and an excess of O in ZnO-NWs.

D. PL Spectrum

Photoluminescence spectra have been acquired on both ZnO-NRs and ZnO-NWs samples in order to investigate the presence of defects. The results obtained for the excitation laser power of 1300 W/m^2 have been reported in Fig. 6.

The spectra have been corrected by taking into account the effect of the substrates, and then they are fitted to multiple Gaussian peaks to identify the UV and VIS components, as shown in Fig. 6. The obtained best fit results are reported in Table II, which shows also the values of the calculated UV/VIS ratio. Actually, the UV/VIS emission intensity ratio is usually taken as an indicator of crystal quality [37], [38], independently on the precise identification of the involved defects and their distribution in the nanostructures.

From Fig. 6, we observe that the PL spectra of both ZnO nanostructures are characterized by an ultraviolet (UV) peak at $\sim$3.3 eV, corresponding to the band edge emission, and by a variety of visible (VIS) bands centred at different energy values and originated by different kinds of defects [10], [34]–[39].

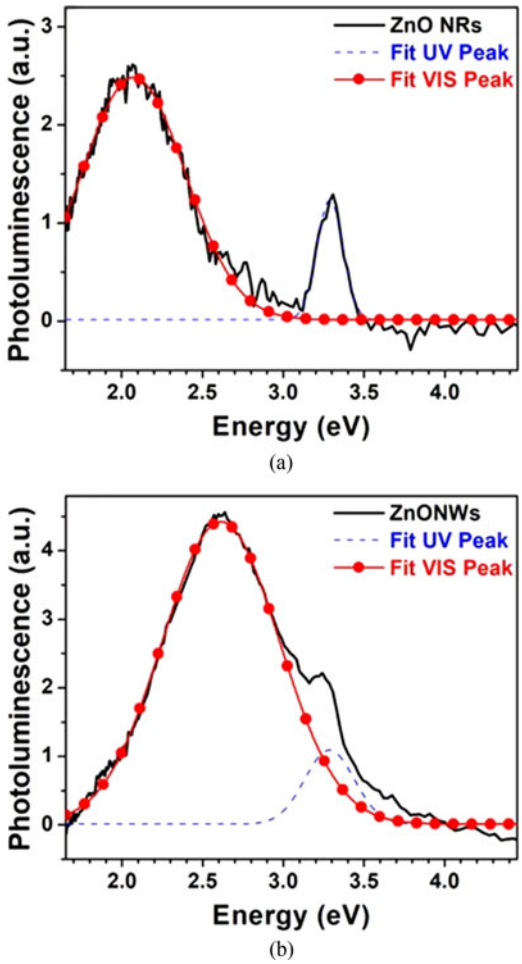

Fig. 6. Photoluminescence spectra of (a) ZnO-NRs and (b) ZnO-NWs. Continuous line represents experimental data corrected for substrate contribution; dashed and dotted line represents Gaussian best fitting results. Both spectra were taken at 1300 W/m^2 excitation power.

TABLE II
BEST FIT RESULTS OF THE ZNO-NRS AND ZNO-NWS PL SPECTRA REPORTED IN FIG. 6

Parameter	NRs		NWs	
	UV	VIS	UV	VIS
Energy (eV)	3.289 ± 0.005	2.075 ± 0.008	3.286 ± 0.008	2.613 ± 0.004
Width (meV)	80 ± 5	330 ± 10	154 ± 8	362 ± 4
Amplit. (a.u.)	12500 ± 700	24500 ± 700	10800 ± 500	44100 ± 300
UV/VIS	0.51 ± 0.08		0.24 ± 0.01	

The UV/VIS Ratio is Calculated from the Amplitude Values of the Gaussian Peaks.

The effect of varying the excitation powers on PL emission was essentially to enhance the UV/VIS intensity ratio for increasing powers; such effect was consistent with the present interpretation of the UV and VIS peaks, as defect-related PL emissions typically tend to saturate at lower excitation powers than band-gap emission (i.e., "intrinsic" emission), since they are limited by the concentration of the defects involved in the recombination. PL peak positions did not show any evident

dependence on PL excitation power, out of the measurements uncertainty.

From Table II, it can be observed that the UV/VIS ratio is higher for ZnO-NRs than for ZnO-NWs, confirming the indications gained from XRD results, which suggested that ZnO-NWs are more defective than ZnO-NRs. Both ZnO-NRs and ZnO-NWs samples have a similar UV peak centred at roughly the same energy, whereas the VIS band is located at $\sim$2.1 eV (yellow band) in the case of ZnO-NRs, and at 2.6 eV (green band) in the case of ZnO-NWs, indicating that different kinds of defects are present in the two materials. The identification of the defects responsible for these two bands is still debated in the current literature, allowing for multiple and controversial interpretations. A definitive assignment of the VIS bands in our samples would require a dedicated study and it is not under the scope of the present work. A possible explanation of the yellow band observed in the ZnO-NRs sample can be attributed to the presence of oxygen vacancies.

A similar interpretation has been recently proposed in the literature [38] for vertically aligned ZnO-NRs. In that work, the authors reported the observation of a PL band around 2 eV, whose intensity decreased after oxygen ions irradiation, and increased with the diameter of the nano-rods, indicating that the defects responsible for that emission involve oxygen vacancies which were localized in the nanorods, within a region up to $\sim$100 nm from their outermost surface. Therefore, since the average diameter of ZnO-NRs is (42 ± 5) nm, we can assume that, according to [38], the oxygen vacancies associated to the yellow PL band are distributed in the whole volume of the nanostructures, resulting in an overall oxygen deficient oxide material. This assumption is supported by XPS and EDX analysis, which indicate a Zn/O ratio > 1.

The green band around 2.5 eV can be linked to zinc vacancies located at the $(10\bar{1}0)$ non-polar surfaces of ZnO nanostructures [39]. Although the cited work does not refer specifically to ZnO nano-walls, its conclusions apply to nanostructures having different morphologies (i.e., ZnO nano-rods and ZnO polycrystalline nanostructured films) provided that there were $(10\bar{1}0)$ non-polar surfaces exposed. In the case of the ZnO-NWs studied in the present work, the morphology showed by AFM is consistent with the presence of unipolar $(10\bar{1}0))$ facets exposed upwards on the sample face, from which the luminescence signal is collected. XRD measurements support the presence of $10\bar{1}0$ facets.

The presence of zinc vacancies in our ZnO-NWs sample is also supported by XPS and EDX analysis, which indicate a Zn/O ratio < 1.

E. Piezoelectric Properties

The piezoelectric coefficient d_{33} of the nanostructured thin films of ZnO-NRs and ZnO-NWs was estimated through PFM. This technique is based on the standard contact mode AFM setup, in which the cantilever and the tip are electrically conductive and an alternating voltage is applied to the conductive tip [18]. Due to the converse piezoelectric effect, the sample responds to the alternating electric field with a periodic deformation. This deformation is detected by the cantilever, through a photodiode. The induced sample displacement Δ_u is related to the amplitude of the applied a.c. voltage V_{ac} through the following expression:

$$\Delta_u = d_{ij}\, V_{ac} \tag{1}$$

in which d_{ij} is the local relevant element of the third-rank piezoelectric tensor of the material [20]. In order to separate the topography and piezoresponse signals, a lock-in amplifier (LIA), which also acts as a sharp band pass filter, is used. The LIA compares the response signal with the reference signal and amplifies only the frequency component that is equal to the reference signal. Since the reference signal and the voltage applied to the tip have the same frequencies, the expected piezoresponse is also at the same frequencies. This allows measurements with a high signal-to-noise ratio, even for small displacements of just a few picometers. The raw amplitude signal, measured using the quadrant photodiode and LIA, is then converted to a displacement amplitude by applying a calibration factor, which is obtained through the measurement of a well-known piezoelectric material. To this purpose, in our study, a Bruker reference sample, consisting of a periodically poled lithium niobate (PPLN) specimen, with an effective piezoelectric coefficient $d_{33\_\mathrm{PPLN}} = 7.5$ pm/V, was employed. In the ideal case the amplitude of the measured piezoresponse A_{piezo} is given by:

$$A_{\mathrm{piezo}} = \alpha\, d_{33}\, V_{ac} \tag{2}$$

in which α is a calibration parameter, d_{33} is the effective piezoelectric coefficient measured via PFM and V_{ac} is the alternating voltage.

In order to estimate α, we applied the background correction technique outlined in [40]. At first, we measured the piezoelectric response of the calibration sample and we estimated the slope m_{PPLN} of the linear fitting of the piezoresponse amplitude versus the applied voltage. Then, we estimated the calibration factor as:

$$\alpha = m_{\mathrm{PPLN}}/d_{33\_\mathrm{PPLN}} \tag{3}$$

in which d_{33_PPLN} is the known piezoelectric coefficient of the reference sample. Finally, we measured the response of the sample under test and we estimated its d_{33} from (2), using the calculated calibration factor α. In the considered test setup, we applied an a.c. voltage to the sample under test, through the tip, and we grounded the bottom electrode.

A comparison of the topographic map and of the PMF-signal map is shown in Fig. 7 for the produced nanostructured films made of ZnO-NRs (Fig. 7(a) and (b)) and of ZnO-NWs (Fig. 7(c) and (d)). The good correlation between morphology and PFM signals of the ZnO-NR sample suggests that the vertical piezoelectric domains are well localized in each single nanorod (Fig. 7(a) and (d)).

On the contrary, the morphology and PFM signals of the ZnO-NW sample are poorly correlated. This is due to the fact that ZnO-NW are not so well vertically oriented with respect to the substrate like the ZnO-NRs, so that the vertical piezoelectric domains are poorly localized.

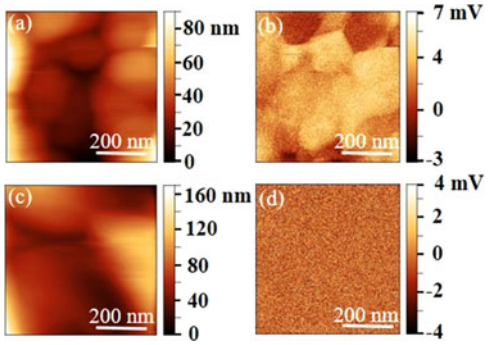

Fig. 7. Typical scanning piezoresponse measurements showing the morphology of (a) ZnO-NRS and (c) ZnO-NWs and the PFM signal for (b) ZnO-NRs and (d) ZnO-NWs.

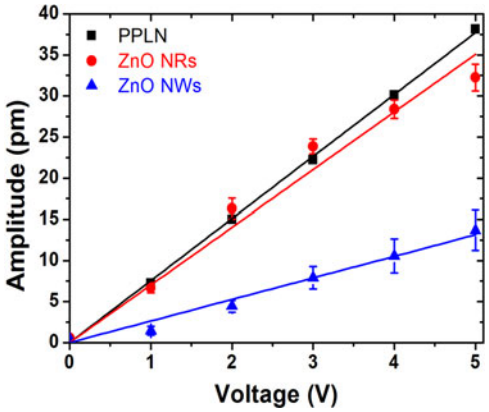

Fig. 8. Measured amplitude of the piezoresponse of different samples with respect to the applied voltage V_{ac}.

TABLE III
PIEZOELECTRIC COEFFICIENT EVALUATED BY AVERAGING THE PFM SIGNAL OVER 3 MEASUREMENT AREAS, $(600 \times 600)\,\mathrm{nm}^2$ IN SIZE

Sample	d_{33} **(pm/V)**
PPLN	7.5
ZnO-NRs	7.01 ± 0.33
ZnO-NWs	2.63 ± 0.49

In order to evaluate the average piezoelectric properties of the samples, PFM measurements were performed over 3 different areas on each sample. Each area has a scanning size of $(600 \times 600)\,\mathrm{nm}^2$, which guarantees a good average signal, as confirmed by the small standard deviations obtained (Fig. 8). As predicted by the theory, the displacement response increases linearly with the driving voltage amplitude. The effective d_{33} was obtained using a linear fit of the amplitude of the average vertical displacement versus the amplitude of the driving voltage, as reported in Fig. 8 for ZnO-NRs and ZnO-NWs. The resulting values of the measured piezoelectric coefficients are reported in Table III.

We noticed a much higher piezoresponse of the ZnO-NR film with respect to the ZnO-NW one. This is due to the different morphology, structural properties and defectiveness of the two nanostructures discussed above. The obtained results are in line with data reported in previous studies [21], [41], which however are focused on a local characterization of the piezoresponse of each single domain or nanostructure. The proposed method instead provides a quantitative estimation of the average value of d_{33}, which is representative of the piezoresponse of the nanostructures material at nanoscale.

IV. CONCLUSIONS

In this paper we reported a comparative study of the properties of 1D (NRs) and 2D (NWs) ZnO-nanostructures, grown by chemical bath deposition (CBD), for potential applications in piezoelectric transduction or energy harvesting. The CBD technique enables a high deposition rate on a wide variety of substrates and over large areas, being also a facile, cost-effective, non-toxic and easy-to scale-up approach.

The piezoelectric properties of the produced samples were investigated through PFM, by scanning different areas of the specimen. We found a piezoelectric coefficient of (7.01 ± 0.33) pm/V for ZnO-NRs and (2.63 ± 0.49) pm/V for ZnO-NWs.

In particular, we correlated the structural, chemical, and morphological properties of the nanostructure with the piezoelectric response of the produced nanostructured thin film.

SEM and AFM analyses confirmed good orientation of the nanostructures and allowed the estimation of their aspect-ratios, i.e., $\sim$4 for ZNO-NRs and $\sim$23 for ZnO-NWs. The XRD spectra confirmed a better crystallinity of ZnO-NRs than of ZnO-NWs. Therefore, ZnO-NRs were characterized by a vertical alignment and a well-defined hexagonal symmetry combined with a good crystallinity (sharp and intense peaks). On the other hand, the XRD data of ZnO-NWs showed an anomalous spread of the (101) peak, which suggests a high defectiveness. The higher defectiveness of ZnO-NWs was also confirmed by PL measurements, highlighting an UV/VIS ratio lower for ZnO-NWs than for ZnO-NRs. The lack of a Bragg reflection at 17.2° in the XRD spectra suggested that sample defectiveness is not related to oxygen vacancies. Vice versa, the position of the centre of the visible PL-band in ZnO-NWs indicated that such defectiveness can be attributed to the presence of zinc vacancies. This result was supported by XPS measurements, which showed a Zn/O ratio < 1, in agreement with the EDX measurements. From XPS measurements we also observed the absorption of water molecules (BE $\approx$ 533 eV), on the surface of ZnO-NRs.

We can conclude that better piezoelectric properties of ZnO-NRs with respect to ZnO-NWs can be related to a combination of the outperforming structural properties, including a better orientation along the *c*-axis, and a lower defectivity of ZnO-NRs over ZnO-NWs. Furthermore, the obtained values of the piezoelectric coefficient, averaged over different areas of the sample surface are representative of the film response and not of the single nanostructure properties. This result suggests that PFM measurements can be employed as a routine test to assess the quality of the piezoelectric nanostructures.

ACKNOWLEDGMENT

We thank Dr. Elisabeth Soergel (Institute of Physics, University of Bonn, Bonn, Germany) for her helpful comments and discussion.

REFERENCES

[1] Z. L. Wang and J. Song, "Piezoelectric nanogenerators based on zinc oxide nanowire arrays," *Science*, vol. 312, pp. 242–246, 2006.

[2] M. Law, L. E. Greene, J. C. Johnson, R. Saykally, and P. Yang, "Nanowire dye-sensitized solar cells," *Nature Mater.*, vol. 4, pp. 455–459, 2005.

[3] R. M. Alenezi, A. S. Alshammari, K. D. G. I. Jayawardena, M. J. Beliatis, S. J. Henely, and S. R. P. Silva, "Role of the exposed polar facets in the performance of thermally and UV activated ZnO nanostructured gas sensors," *J. Phys. Chem. C*, vol. 117, pp. 17850–17858, 2013.

[4] Z. L. Wang and W. Wu, "Nanotechnology-enabled energy harvesting for selfpowered micro-/nanosystems," *Angewandte Chemie, Int. Edition*, vol. 51, pp. 11700–11721, 2012.

[5] K. Savarimuthu, G. Rajamanickam, R. Shankararajan, R. Perumal, and A. Rayarfrancis, "Experimental study on flexible ZnO based nanogenerator using schottky contact for energy harvesting applications," *IEEE Trans. Nanotechnol.*, vol. 16, no. 3, pp. 469–476, May 2017.

[6] C. Besleaga, G. Stan, A. Galca, L. Ion, and S. Antohe, "Double layer structure of ZnO thin films deposited by RF-magnetron sputtering on glass substrate," *Appl. Surf. Sci.*, vol. 258, pp. 8819–8824, 2012.

[7] E. Zanni *et al.*, "In vitro toxicity studies of zinc oxide nano- and microrods on mammalian cells: A comparative analysis," *Mater. Lett.*, vol. 179, pp. 90–94, 2016.

[8] D. Bekermann *et al.*, "ZnO Nanorod arrays by plasma-enhanced CVD for light-activated functional applications," *Chem. Phys. Chem.*, vol. 11, pp. 2337–2340, 2010.

[9] C. C. Lin and Y. Y. Li, "Synthesis of ZnO nanowires by thermal decomposition of zinc acetate dihydrate," *Mater. Chem. Phys.*, vol. 113, pp. 334–337, 2009.

[10] C. R. Chandraiahgari *et al.*, "Synthesis and characterization of ZnO nanorods with a narrow size distribution," *RSC Adv.*, vol. 5, no. 62, pp. 49861–49870, 2015.

[11] B. Cao and W. Cai, "From ZnO nanorods to nanoplates: Chemical bath deposition growth and surface-related emissions," *J. Phys. Chem. C*, vol. 112, no. 3, pp. 680–685, 2008.

[12] V. Strano *et al.*, "Double role of HMTA in ZnO nanorods grown by chemical bath deposition," *J. Phys. Chem. C*, vol. 118, pp. 28189–28195, 2014.

[13] G. Yi, C. Wang, and W. I. Park, "ZnO nanorods: synthesis, characterization and applications," *Semicond. Sci. Technol.*, vol. 20, pp. S22–S34, 2005.

[14] C. Falconi, G. Mantini, A. D'Amico, and Z. L. Wang, "Studying piezoelectric nanowires and nanowalls for energy harvesting," *Sensors Actuators, B, Chem.*, vol. 139, pp. 511–519, 2009.

[15] S. S. Warule, N. S. Chaudhari, B. B. Kale, and M. A. More, "Novel sonochemical assisted hydrothermal approach towards the controllable synthesis of ZnO nanorods, nanocups and nanoneedles and their photocatalytic study," *Cryst. Eng. Commun.*, vol. 11, pp. 2776–2783, 2009.

[16] P. Rai, S. Raj, I.-H. Lee, W.-K. Kwak, and Y.-T. Yun, "Conversion of ZnO microrods into microdisks like structures and its effect on photoluminescence properties," *Ceram. Int.*, vol. 39, pp. 8287–8291, 2013.

[17] J.-M. Liu, B. Pan, H. Chan, S. Zhu, Y. Zhu, and Z. Liu, "Piezoelectric coefficient measurement of piezoelectric thin films: an overview," *Mater. Chem. Phys.*, vol. 75, pp. 12–18, Apr. 2002.

[18] E. Soergel, "Piezoresponse Force Microscopy (PFM)," *J. Phys. D, Appl. Phys.*, vol. 44, 2011, Art. no. 464003.

[19] A. Kholkin, S. Kalinin, A. Roelofs, and A. Gruverman, *Scanning Probe Microscopy: Electrical and Electromechanical Phenomena at the Nanoscale*. New York, NY, USA: Springer, 2006.

[20] D. Denning, J. Guyonnet, and B. J. Rodriguez, "Applications of piezoresponse force microscopy in materials research: From inorganic ferroelectrics to biopiezoelectrics and beyond," *Int. Mater. Rev.*, vol. 61, pp. 46–70, 2016.

[21] D. Tamvakos *et al.*, "Piezoelectric properties of template-free electromechemically grown ZnO nanorod arrays," *Appl. Surf. Sci.*, vol. 356, pp. 1214–1220, 2015.

[22] H. Fan *et al.*, "Template-assisted large-scale ordered arrays of ZnO pillars for optical and piezoelectric applications," *Small 2*, vol. 2, pp. 561–568, 2006.

[23] C. R. Chandraiahgaria *et al.*, "Control of size and density of ZnO-nanorods grown onto graphene nanoplatelets in aqueous suspensions," *RSC Adv.*, vol. 1, pp. 1–3, 2016.

[24] H. Sowa and H. Ahsbahs, "High-pressure X-ray investigation of zincite ZnO single crystals using diamond anvils with an improved shape," *J. Appl. Crystallography*, vol. 39, no. 39, pp. 169–175, 2006.

[25] M. Di Marco, M. Port, P. Couvreur, C. Dubernet, P. Ballirano, and C. Sadun, "Structural characterization of ultrasmall superparamagnetic iron oxide (USPIO) particles in aqueous suspension by energy dispersive x-ray diffraction (EDXD)," *J. Amer. Chem. Soc.*, vol. 126, pp. 10054–10059, 2006.

[26] M. Di Marco *et al.*, "Atomic Pair Distribution Function (PDF) study of iron oxide nanoparticles in aqueous suspension," *J. Mater. Chem.*, vol. 19, pp. 6354–6360, 2009.

[27] P. Ballirano, C. De Vito, V. Ferrini, and S. Mignardi, "The thermal behaviour and structural stability of nesquehonite, $Mg_2CO_3 \cdot 3H_2O$, evaluated by in situ laboratory parallel-beam X-ray powder diffraction: New constraints on CO_2 sequestration within minerals," *J. Hazardous Mater.*, vol. 178, pp. 522–528, 2010.

[28] A. Katerinopoulou, T. Balic-Zunic, and L. F. Lundegaard, "Application of the ellipsoid modeling of the average shape of nanosized crystallites in powder diffraction," *J. Appl. Crystallography*, vol. 45, no. 45, pp. 22–27, 2012.

[29] I. Kaurova, G. Kuzmicheva, and V. Rybakov, "Growth and structural, optical, and electrical properties of zincite crystals," *Crystallography Rep.*, vol. 58, pp. 226–233, 2013.

[30] J. F. Moulder, W. F. Stickle, P. E. Sobol, and K. D. Bomben, *Handbook of X-ray Photoelectron Spectroscopy*. 2nd ed. Eden Prairie, MN, USA: Physical Electronics, 1992.

[31] D. Barreca, A. Gasparotto, C. Maccato, C. Maragno, and E. Tondello, "TiO_2 thin films by chemical vapor deposition: An XPS characterization," *Surf. Sci. Spectra*, vol. 14, pp. 27–33, 2007.

[32] S. Kaciulis *et al.*, "Nanowires of metal oxides for gas sensing applications," *Surf. Interface Anal.*, vol. 40, pp. 575–578, 2008.

[33] S. Kaciulis, G. Mattogno, A. Galdikas, A. Mironas, and A. Setkus, "Influence of surface oxygen on chemoresistance of tin oxide film," *J. Vac. Sci. Technol. A*, vol. 14, pp. 3164–3168, 1996.

[34] A. B. Djurisic *et al.*, "Green, yellow, and orange defect emission from ZnO nanostructures: Influence of excitation wavelength," *Appl. Phys. Lett.*, no. 88, 2006, Art. no. 103107.

[35] Y. W. Heo and S. J. Pearton, "Origin of green luminescence in ZnO thin film grown by molecular-beam epitaxy," *J. Appl. Phys.*, vol. 98, 2005, Art. no. 073502.

[36] Y. Y. Tay *et al.*, "Correlation between the characteristic green emissions and specific defects of ZnO," *Phys. Chem. Chem. Phys.*, vol. 12, pp. 2373–2379, 2010.

[37] I. Shalish, H. Temkin, and V. Narayanamurti, "Size-dependent surface luminescence in ZnO nanowires," *Phys. Rev. B, Condens. Matter Mater. Phys.*, vol. 69, 2004, Art. no. 245401.

[38] S. Jiang *et al.*, "Tunable photoluminescence properties of well-aligned ZnO nanorod array by oxygen plasma post-treatment," *Appl. Surf. Sci.*, no. 289, pp. 252–256, 2014.

[39] F. Fabbri *et al.*, "Zn vacancy induced green luminescence on non-polar surfaces in ZnO nanostructures," *Sci. Rep.*, vol. 4, 2014, Art. no. 5158.

[40] T. Jungk, A. Hoffmann, and E. Soergel, "Quantitative analysis of ferroelectric domain imaging with piezoresponse force microscopy," *Appl. Phys. Lett.*, vol. 89, 2006, Art. no. 163507.

[41] M. K. Gupta, J.-H. Lee, K. Y. Lee, and S.-W. Kim, "Two-dimensional vanadium-doped ZnO nanosheet-based flexible direct current nanogenerator," *ACS Nano*, vol. 7, pp. 8932–8939, 2013.

Marco Fortunato (M'16) received the Bachelor's degree in physics from the Sapienza University of Rome, Rome, Italy, in 2011 and the Master's degree in physics of condensed matter from the Roma Tre University of Rome, Rome, Italy, in 2015. Since November 2015, he has been working toward the Ph.D. degree at the Department of Astronautical, Electrical, Energy Engineering, in the Research Center for Nanotechnology Applied to Engineering, Sapienza University of Rome. His current research interests include characterization of piezoelectric material with AFM and PFM for energy harvesting application.

Chandrakanth Reddy Chandraiahgari received the BSc. degree in physics and electronics from Kakatiya University, Warangal, India, in 2006, the M.Sc. degree in applied electronics from Osmania University, Telangana, India, in 2009, the "Erasmus Mundus" M.S. dual degree in nanoscience and nanotechnology from Katholieke Universiteit Leuven, Leuven, Belgium and Chalmers University of Technology, Gothenburg, Sweden, in 2011 and the Ph.D. degree in energy engineering from the Sapienza University of Rome, Rome, Italy in 2015. His research interests include large scale synthesis of ZnO and graphene hybrid nanostructured materials for energy and environment applications.

Giovanni De Bellis (M'12) received the Laurea degree in materials engineering and the Ph.D. degree in electrical engineering, both from the Sapienza University of Rome, Rome, Italy. He is currently an Assistant Professor of electrical engineering with the Department of Astronautical, Electrical and Energy Engineering, Sapienza University of Rome. His main research interests include graphene-based nanomaterials, electromagnetic absorbing and shielding materials, and strain sensors.

Paolo Ballirano received the Laurea (summa cum laude) and Ph.D. degrees in geological sciences from the Sapienza University of Rome, Rome, Italy, in 1990 and 1994, respectively. Since 2016, he has been a Full Professor of mineralogy with the Faculty of Mathematical, Physical, and Natural Sciences, Sapienza University of Rome, Rome, Italy. He is currently the Director with the Department of Earth Sciences of Sapienza. He has authored or coauthored more than 120 papers in the field of mineralogy, materials science, physical chemistry, and crystallography. His research interests include definition of the correlations existing between physical-chemical properties and toxicity of mineral fibers.

Peiman Soltani received the B.Sc. degree in mechanical engineering in the field of heat and fluids from the University of Shahrekord, Shahrekord, Iran, in 2010 and the M.Sc. degree in mechanical engineering in the field of applied design from the Isfahan University of Technology, Isfahan, Iran, in 2012. Since November 2014, he has been working toward the Ph.D. degree at the Department of Industrial Engineering, Rome, Italy. His research interests include application of surface analysis on innovative materials such as LDHs, graphene based materials, etc.

Saulius Kaciulis received the Graduate degree in physics and the Ph.D. degree in semiconductor physics from the University of Vilnius, Vilnius, Lithuania, in 1977 and 1983, respectively. From 1976 to 1997, he has been employed with the Semiconductor Physics Institute in Vilnius. Since 1985, he started to specialize in the techniques of solid-state surface analysis: XPS, AES, SIMS, etc. From 1992 to 1996, he was a Visiting Professor with the Institute of Materials Chemistry, National Research Council (CNR), Italy. Since 1997, he has been a Senior Researcher with the Institute for the Study of Nanostructured Materials, CNR, Rome, Italy. He has coauthored more than 200 scientific papers. His research interests include surface analysis and depth profiling of innovative materials: thin films and heterostructures, corrosion-resistant coatings, biocompatible materials, nanostructured, and 2-D materials. He is a Member of the International Advisory board of ECASIA, of the Editorial board of the journal Surface Interface Analysis (Wiley, U.K.) and the committee of Italian Association of Metallurgy.

Luisa Caneve received the degree in physics from the University of Rome "La Sapienza," Rome, Italy. Since 1989, she has been a Senior Scientist with ENEA, the Italian National Agency for New Technologies, Energy and Sustainable Economic Development. Experience on laser-matter interaction processes with particular attention on the development of spectroscopic techniques by laser. In this field, research activities on study and development of laser induced breakdown spectroscopy and laser induced fluorescence for several applications, from the environmental monitoring and artwork conservation to energy and security. Involved in several national and international research projects in these different fields. She has published more than 50 international journals and proceedings of national and international conferences.

Francesca Sarto received the Laurea degree in physics from the University of Rome " La Sapienza," Rome, Italy, in 1992, the Ph.D. degree in industrial engineering from the University of Rome Tor Vergata, Rome, Italy. She is currently a Senior Scientist with ENEA, the "Italian Agency for New Technologies, Energy and Sustainable Economic Development", where she has been working since 1993 on thin films technologies, and nanostructured material characterization, for optical and energetic applications. In the context of her research activity, she participated to national and international projects and she was author of more than 70 scientific papers and 5 patents. Her research interests include photoluminescence spectroscopy, zinc oxide, multifunctional coatings, and fuel cell catalysts.

Maria Sabrina Sarto (F'10) received the Laurea (summa cum laude) and Ph.D. degrees in electrical engineering from the Sapienza University of Rome, Rome, Italy, in 1992 and 1997, respectively. Since 2005, she has been a Full Professor of electrotechnics, electromagnetic compatibility, and nanotechnology with the Faculty of Engineering, Sapienza University of Rome, Rome, Italy, where she has been also the Director of Research Center on Nanotechnology Applied to Engineering, from 2006 to 2015. She is currently the Director with the Department of Astronautics, Electrical and Energy Engineering of Sapienza, Rome, Italy, and the Deputy Rector for Research Infrastructures. She has authored or coauthored more than 160 papers in the field of EMC, nanotechnology, and advanced nanomaterials. Her current research interests include carbon nanomaterial and graphene base polymer composites, graphene-based nanomaterials for EMC applications, sensors, and radar absorber.